ESAIM: PROCEEDINGS, February 2007, Vol.16, 51-65
Eric Cancès & Jean-Frédéric Gerbeau, Editors
DOI: 10.1051/proc:2007009

SHOCK-INDUCED NOISE IN 2D SUB- AND SUPERSONIC MIXING LAYERS

J. Schulze[1], Ch. Schaupp[1], J. Sesterhenn[1], R. Friedrich[1], J. Berland[2], Ch. Bogey[2] and D. Juvé[2]

Abstract. A numerical code solving acoustic analogies to predict shock-induced noise is developed. Both Lighthill's analogy and the one of Ffowcs-Williams and Hawkings (FWH) are implemented and compared to the acoustic far field of the direct numerical simulation (DNS) in detail. In addition to this the linearized Euler Equations (LEE) are used to propagate into the acoustic far field and the results are also compared to the DNS-data. With a two dimensional mixing layer in a subsonic test case and a Reynolds number based on the initial shear layer thickness $Re_{\delta_\omega^0}$ of $1.42 \cdot 10^5$, a first application of the code is performed. To investigate the shock-induced noise, a two dimensional supersonic mixing layer with an impinging oblique shock is simulated. The results of the analogies for the shock-induced noise are in good agreement with the acoustic far field of the DNS. The accuracy of the FWH-method is better than the one of Lighthill's analogy.

1. Introduction

Understanding and predicting the sound generation processes by supersonic turbulent jets issuing for example from the exhaust of civil and military aircraft is an issue of great interest: Reduction of noise, polluting the environment is desired and minimization of damage to engine or nozzle parts due to high-intensity sound radiated by the jet flow is necessary.

The supersonic jets considered here are either over- or underexpanded. Thus, a shock-cell structure exists within the jet core, which gives rise to additional noise components, to be investigated here: Shock–associated noise and jet screech.

Different approaches to numerical simulation of noise generation within these jet flows have been adopted by the participants of this research project, conducted within the framework of CEMRACS 2005. While the French group from École Centrale de Lyon focused on Large-eddy simulation of a planar, supersonic jet subject to the screech phenomenon, the German participants from Technische Universität München performed DNS of the isolated planar mixing layer–compression wave interaction.

In this way, it was possible on the one hand to capture the complete near acoustic field including mixing noise, shock-associated noise and jet screech, and to demonstrate the capabilities of the LES method to handle problems of this kind. On the other hand, the sound generation by interaction of turbulence with the oblique compression/expansion structures, which is of fundamental importance within the phenomena of shock-associated noise and jet screech, could be investigated in detail.

The CEMRACS 2005 event with a focus on computational aeroacoustics offered an excellent opportunity to define and perform joint work related to the supersonic jet noise problem. Propagation of sound computed by

[1] Technische Universität München, Germany
[2] École Centrale de Lyon, France

DNS/LES close to the jet or the mixing layer, respectively, into the far acoustic field was selected as focus of our work during CEMRACS 2005. Different approaches to far field sound propagation have been applied to the oblique shock/shear layer interaction case; the methods used (propagation by Lighthill's analogy, Ffowcs-Williams and Hawkings analogy and linearized Euler equations) and the results obtained shall be presented in the following.

2. Governing theory

In this section, Lighthill's analogy and the FWH-method are presented. For both analogies the numerical procedure is explained in detail. The used LEE-method is described at the end of this chapter.

2.1. **Lighthill's Analogy**

Lighthill's [24] 1951 idea was to make a rearrangement of the compressible and unsteady Navier-Stokes (NS) equations into an inhomogeneous wave equation without any approximations or modeling. The right hand side of the new found wave equation can now be interpreted as acoustic source term called Lighthill's source:

$$\frac{\partial^2 \rho'}{\partial t^2} - c_0^2 \Delta \rho' = \frac{\partial^2 T_{ij}}{\partial x_i \partial x_j} \tag{2.1}$$

where c_0 is the ambient speed of sound and T_{ij} is Lighthill's stress tensor defined as:

$$T_{ij} = \rho u_i u_j + (p' - \rho' c_0^2)\delta_{ij} - \tau_{ij}; \tag{2.2}$$

primed variables denote fluctuations like $p' = p - p_0$. Far away from the turbulent aerodynamic field the tensor T_{ij} disappears and can be set to zero. So the sources only play a role in a limited volume including the turbulent fluctuations. As estimated by Goldstein [20] and Lighthill [24] the dominant part of the sources are the Reynolds stresses $\rho u_i u_j$. Unlike most articles in the literature, where the other two parts of the tensor T_{ij} are neglected, we will use the complete source, since the deviation of the isentropic behavior $(p' - \rho' c_0^2)\delta_{ij}$ plays a role for supersonic cases.

2.1.1. *Numerical algorithm*

The solution of Lighthill's equation is obtained using the three dimensional free space Green's function. It can be written for space derivatives of Lighthill's stress tensor in the following form:

$$p'(\vec{x}, t) = \frac{1}{4\pi} \int_V \frac{1}{r} \frac{\partial^2 T_{ij}}{\partial y_i \partial y_j} \left(\vec{y}, t - \frac{r}{c_0} \right) \mathrm{d}\vec{y}. \tag{2.3}$$

where $r = |\vec{x} - \vec{y}|$ is the distance between the observer's location $\vec{y}$ and the the source $\vec{x}$. V is the volume including all relevant acoustic sources. These sources have to be evaluated at the retarded time $\tau = t - \frac{r}{c_0}$ which makes interpolation between stored time steps necessary. This method was also used in [6] and differs from the method used in [34], where a Green's function in frequency space is used to avoid interpolation in time.

Interpolation. The interpolation is performed using Lagrange polynomials (fourth-order) or, depending on the case, WENO interpolation [26] (first- to sixth-order), if the sources show strong discontinuities in time. It is very important to choose the right interpolation scheme, because an unfavorable interpolation of the sources at the retarded time can cause a high frequency noise in the acoustic far field. In addition to this the recording time step has to be small enough to take into account all oscillations of the source in order to guarantee a physical "correct" reconstruction of the source-term. In the present study a fourth-order WENO-interpolation is used for most cases.

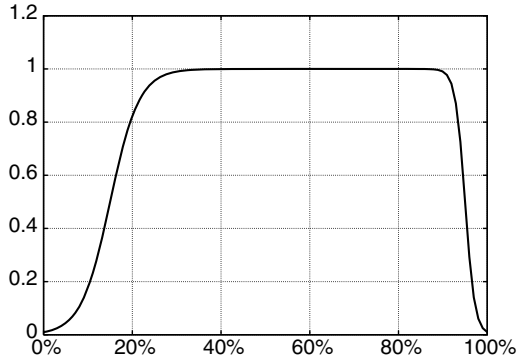

FIGURE 1. Implemented window function; Example: inlet: 33%, outlet: 10%

Low-pass filtering. If the temporal resolution of the sources is too small (due to storage used), a low-pass filtering of Lighthill's sources can avoid high frequency noise in the far field. In the present study a Butterworth low-pass filter was used to adjust temporal badly resolved sources. It has to be mentioned that the filtering of the source only reduces the high frequency noise but is not effecting a better solution.

Integration. Subsequent to the interpolation, the sources are integrated over the source volume V. The integration is approximated with the midpoint rule, which is a simple but fast method. An application of a method with a higher resolution, like the Simpson rule, is by reason of the later explained "QuickSort"-method not such straightforward.

Window function. Most technical applications make it impossible to locate all sources in a closed volume; e.g. in a jet a convective flow transports the sources through a fixed volume. It is therefore essential to add special inflow and outflow conditions to the near field. Otherwise noise from the region of the in- and outlet would cover the far field. In the present study, a window function fades the sources slowly in the near field and out on the outlet. It consists of two hyperbolic tangent functions and can be defined by:

$$\begin{aligned} f(x) &= \frac{1}{2}\Big[\tanh\left(2(x - x_{start} - \frac{b_v}{2})\right)\frac{1}{b_v} \\ &\quad - \tanh\left(2(x - x_{end} + \frac{b_h}{2})\right)\frac{1}{b_h}\Big] \end{aligned} \tag{2.4}$$

where the parameters b_i, $i = v, h$ modify the width of the window in- and outlet. These parameters have to be adjusted carefully for each case. It could be shown that the width of the window in- and outlet has to be at least as large as the distance of two convecting acoustic sources (e.g. vortices). In fig. 1 an example of a possible window function is presented.

Averaging. As described for example in Bogey et al. [6], it is necessary to calculate and subtract the average of the sources in order to obtain a centered pressure fluctuation. The new found source term is obtained by:

$$\frac{\partial^2 T_{ij}}{\partial x_i \partial x_j}^{*} = \frac{\partial^2 T_{ij}}{\partial x_i \partial x_j} - \overline{\frac{\partial^2 T_{ij}}{\partial x_i \partial x_j}}. \tag{2.5}$$

The temporal average is thereby calculated over the sum of all stored time steps divided by their number:

$$\overline{\frac{\partial^2 T_{ij}}{\partial x_i \partial x_j}} \approx \sum_{z=1}^{N} \frac{\partial^2 T_{ij}}{\partial x_i \partial x_j}|_z / N, \tag{2.6}$$

Mean-flow interaction. In many technical applications the sound of the sources is emitted in a medium with a more or less uniform motion (e.g. a jet engine, where the sound is emitted in a medium with the speed of the

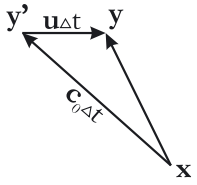

FIGURE 2. Schematic view of the flow situation in the far field with a moving medium (velocity u).

aircraft, propelled by the jet engine). For this case the free space Green's function has to be adjusted to take the mean-flow effects into account. If the medium in the acoustic far field is not at rest the velocity of propagation of the acoustic waves is no more uniform in all directions, but a vectorial sum of all concerned velocities. An observer in an upstream direction of a source would hear their signal later than an observer in flow direction. According to this a mean-flow in the far field also affects the retarded time ($\tau = \tau(c)$).

The problem can be formulated in vectorial notation:

$$\vec{c}_0 \Delta t + \vec{u} \Delta t - \vec{r} = \vec{0}, \tag{2.7}$$

where Δt denotes the runtime of a signal from the source $\vec{x}$ to the far field $\vec{y}$ with the virtual observer location $\vec{y}'$ (see fig. 2).

In order to reduce the problem, the following simplifications are used:

- $\vec{u} = (u_1, 0, 0)^T$; parallel mean-flow
- $\vec{r} = (r_1, r_2, 0)^T$; two-dimensional problem

The new found retarded time $\tau^* = t - \Delta t$ can now be determined to:

$$\tau^* = t - \frac{1}{c_0 \left(M_s^2 - 1\right)} \left(M_s \Delta x - \sqrt{M_s^2 \Delta x^2 + r^2} \right), \tag{2.8}$$

with the Mach number M_s of the parallel flow in the far field and $\Delta x = x_1 - y_1$. Equation (2.8) has to be inserted in a modified Green's function:

$$p'(\vec{x}, t) = \frac{1}{4\pi |1 + M_s \frac{\Delta x}{r}|} \int_V \frac{1}{r} \frac{\partial^2 T_{ij}}{\partial y_i \partial y_j} (\vec{y}, \tau^*) \, \mathrm{d}\vec{y}. \tag{2.9}$$

Numerical issues. The solution of Lighthill's analogy with Green's function needs the information of the acoustic sources stored over a certain period of time in order to evaluate the sound in a far field with a certain size. To calculate the acoustic fluctuation at one point in the far field, all this point's affecting sources have to be taken into account. The calculation of more than one point (a field) makes it necessary to read each saved time step more than once which is temporal expensive. In the present code all existing retarded times ($n_{\text{ret.times}} = n_{\text{nearfield}} \cdot n_{\text{farfield}} \sim 10^9$, for an average 2D problem) are sorted by their length to recognize which source emits its signal in a certain interval of time. This interval is defined by the interpolation procedure (e.g. a Lagrange-polynomial of fourth-order uses a stencil with five nodes, so the interval could be placed between the first and fifth node). In the present study the interval for the fourth-order Lagrange interpolation is placed between the second and third interpolation value. So the interval has a length of $2 \cdot \Delta t$ if the time step is equidistant (this is not a mandatory condition). For the WENO interpolation the length of the interval is set to $1 \cdot \Delta t$ and placed in the middle of the stencil (depending on the order). By reading one stencil respectively (e.g. five sequenced time steps), which defines an interpolation interval, a repeated reading of the saved sources is avoided. Implemented is the fast QuickSort algorithm [21].

2.2. **Ffowcs-Williams and Hawkings Analogy**

Most of the above mentioned numerical issues are not necessary for the Ffowcs-Williams and Hawkings method. The FWH-equation is based on Lighthill's analogy and represents an advanced Lighthill-equation. Again, the FWH-equation is a rearrangement of the compressible NS-equations and includes a source term on their right hand side. Unlike Lighthill's method, the sources are not stored in a closed volume with all the turbulent fluctuations but on a surface surrounding all acoustic sources and, in addition to this, in the area outside this surface (T_{ij}). In most cases, the FWH-equation is applied to problems with moved bodies like the sound radiation of a rotor blade. For this case the sources have to be taken into account on the surface of the rotor blade and in the surrounding medium (vortices caused by the rotor blade). It is needles to say that the sources surrounded by the surface - in our case the sources *in* the rotor blade - have to be set to zero. If one tries to predict the radiated sound of a free jet, no solid surfaces are present. The surface, on which a part of the FWH-sources are stored, can now be chosen arbitrary. It is however useful to choose a surface which surrounds all the turbulent fluctuations because all the sources T_{ij} are zero outside the volume and, as aforementioned, have to be zero in the volume, also. In this case, only sources on a surface remain and the volume integration in Lighthill's analogy turns into a surface integration for the FWH-equation which reduces the computational costs drastically. It has to be mentioned that these FWH-sources are based on acoustic fluctuations in the acoustic far field and not on noise generating turbulent fluctuations in the near field as they are the basis for Lighthill's analogy.

The FWH-equation in integral notation, for a free jet with no solid surfaces, is obtained by:

$$\begin{aligned} 4\pi\{p'(\vec{x},t)\cdot H(f)\} = &\frac{\partial}{\partial t}\int\limits_S \left(\frac{\rho u_i}{r}n_i\right)_\tau \mathrm{d}S \\ &-\frac{\partial}{\partial x_i}\int\limits_S \left(\frac{\rho u_i u_j + P_{ij}}{r}n_j\right)_\tau \mathrm{d}S, \end{aligned} \tag{2.10}$$

with $P_{ij} = p'\delta_{ij} - \tau_{ij}$ and the Heaviside-function $H(f)$ which is zero in the area surrounded by the the surface S. The index τ indicates that the sources have to be evaluated at the retarded time, whereas the retarded time can be calculated by eq. (2.8) to take mean flow effects into account. In comparison to Lighthill's analogy the FWH-sources are not a scalar but a symmetric matrix which increases the amount of storage about the sixfold. This source-matrix is multiplied by the normal vector n_i of the surface and then interpolated at the retarded time. The interpolation scheme can be adopted from the Lighthill analogy whereas the integration has to be reduced to a surface integration. All other numerical issues, like the window-function or the averaging and filtering of the sources, are unnecessary for the FWH-method.

2.3. **Far-field sound propagation using LEE**

A hybrid zonal approach can be implemented to predict the far-field noise. In this approach, the near-field data provided by the DNS computation is extrapolated using a simplified set of equations, allowing long-range propagation of acoustic waves.

In the present work, the two-dimensional linearized Euler Equations (LEE) are solved beyond an extrapolation line, which is specified by the DNS near-field. Assuming that time-dependent perturbations are small, and keeping only the first order terms in the Euler equations yields the LEE, given in two dimensions by,

$$\frac{\partial \mathbf{U}'}{\partial t} + \frac{\partial \mathbf{E}'}{\partial x} + \frac{\partial \mathbf{F}'}{\partial y} + \mathbf{H}' = 0 \tag{2.11}$$

where,

$$\mathbf{U}' = [\rho', \rho_0 u', \rho_0 v', p'] \tag{2.12}$$
$$\mathbf{E}' = [\rho' u_0 + \rho_0 u', \rho_0 u_0 u' + p', \rho_0 u_0 v', u_0 p' + \gamma p_0 u'] \tag{2.13}$$
$$\mathbf{F}' = [\rho' v_0 + \rho_0 v', \rho_0 v_0 u', \rho_0 v_0 v' + p', v_0 p' + \gamma p_0 v'] \tag{2.14}$$

The term $\mathbf{H}'$, defined as,

$$\mathbf{H}' = [0, (\rho_0 \mathbf{u}' + \rho' \mathbf{u_0}) \cdot \nabla u_0, (\rho_0 \mathbf{u}' + \rho' \mathbf{u_0}) \cdot \nabla v_0, (\gamma - 1) p' \nabla \cdot \mathbf{u}' - (\gamma - 1) \mathbf{u}' \cdot \nabla p_0] \tag{2.15}$$

takes into account the mean flow inhomogeneities, with $\mathbf{u}' = (u', v')$ and $\mathbf{u_0} = (u_0, v_0)$. The specific heat ratio γ is equal to 1.4.

The LEE are solved using the low dispersive and low dissipative explicit numerical algorithms developed by Bogey & Bailly [9]: optimized eleven-point finite differences are implemented to compute spatial derivatives, and selective filtering is performed with optimized eleven-point filter. Time integration is carried out by an optimized fourth-order six-stage low-storage Runge-Kutta scheme [4]. The non-reflecting boundary conditions of Tam & Dong [43] are implemented to model a free-field space. More details on the extrapolation procedure are provided in [5], where LEE are used to propagate screech tones predicted by LES into the far-field.

3. Application

In this chapter, numerical results of the *Lighthill/FWH*-code and the *LEE*-code for two application cases are presented. These are:

(1) Subsonic mixing layer (both velocities subsonic); computed with Lighthill's analogy (two-dimensional computation).
(2) Supersonic mixing layer interacting with an oblique shock; computed with Lighthill's analogy, the FWH method and LEE-propagation (two-dimensional computation).

To save computational time, the used DNS cases are simulated in a two-dimensional domain. It has to be mentioned that in these idealized two-dimensional computations the acoustic source diverges from a real three-dimensional case. As a consequence, effects like the roll up and pairing of vortices might be stronger and lead to a raised acoustic noise level. For a detailed description of the used DNS cases see [37].

3.1. Subsonic mixing layer

The subsonic mixing layer is forced with its most unstable frequency f_0 and its first sub-harmonic, in order to achieve a vortex pairing at a more or less fixed location. This vortex pairing is the dominant acoustic source in this test case and emits an acoustic signal with the frequency of the vortex pairing ($f_P = f_0/2$). Michalke [28] showed with a linear stability analysis that this frequency can be determined to:

$$f_0 = 0.132 \frac{u_c}{\delta_\omega^0}, \tag{3.16}$$

with the common velocity $u_c = (u_1 + u_2)/2$ and the initial mixing layer thickness δ_ω^0. The parameters of the DNS for this test case are listed in tab. 1.

A result of the DNS (near field) for the vorticity and the divergence of Lighthill's stress tensor (acoustic source) is shown in fig. 3, where the x-location of the vortex pairing seems to be around $x = 90 \cdot \delta_\omega^0$. This point is the origin of the dominant acoustic source. In fig. 4 the *Lighthill*-solution for this first test case is presented. For this calculation, mean-flow interactions (eq. (2.8)) are taken into account.

The excepted sound with a wavelength of $\lambda_P = 50.1 \delta_\omega^0$ is clearly visible in the far field but also a high frequency noise with no physical meaning. Their origin might be the interpolation procedure, since it is emitted from nearly every point in the near field. A cut through the far field in y-direction is shown in fig. 5 where

Case			I
u_1	$0.4c_0$	L_x/δ^0_ω	346
u_2	$0.2c_0$	L_y/δ^0_ω	157
μ_0	$1.824 \cdot 10^{-5} \frac{kg}{m \cdot s}$ (Air)	n_x	512
$\mathrm{Re}_{\delta^0_\omega}$	$1.42 \cdot 10^5$	n_y	384

Table 1. Parameter of the DNS for the subsonic mixing layer (test case one)

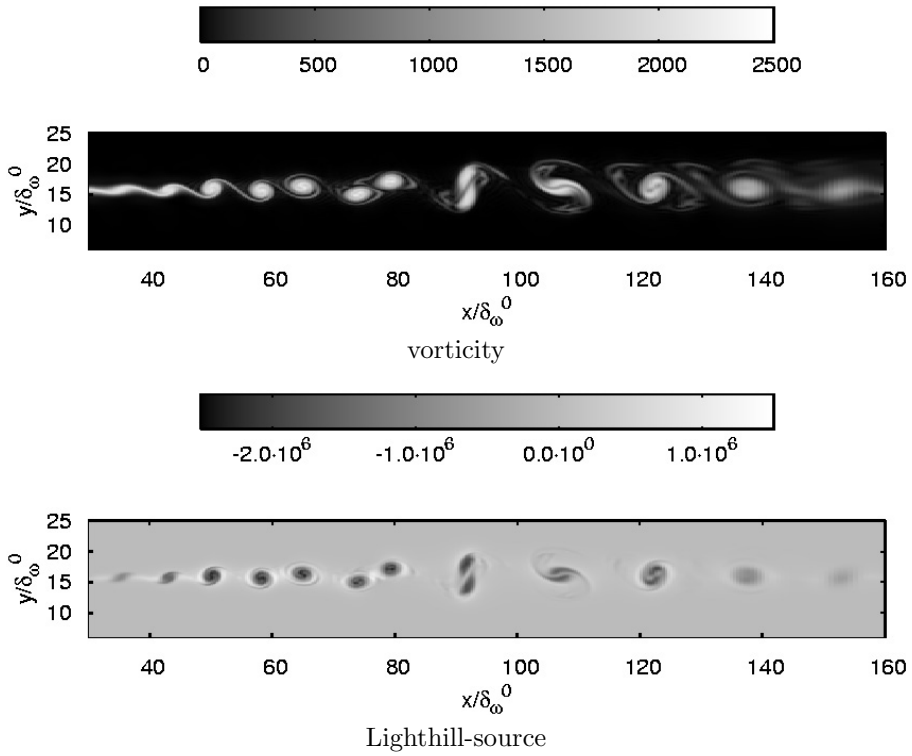

Figure 3. Subsonic mixing layer; *top*: vorticity; *bottom*: divergence of Lighthill's stress tensor

the emitted sound but also the noise is visible more detailed (including the filtered case; see the following paragraph).

In order to reduce the noise in the far field, the Lighthill sources are filtered in time with a low-pass Butterworth filter at a cutoff-frequency of $f_{cut} = 2.5 f_P = 5.0 f_0$. Through the application of the filtering, the noise in the far field of the *Lighthill*-solution could be reduced but also the amplitude of the acoustic waves is reduced. In fig. 5 a cut through the far field is shown for both the filtered and the unfiltered case.

The influence of the parameters of the window function is demonstrated in fig. 6, with a series of snapshots of a small part of the far field. Modified is the width of the window function at the inlet, while the width of the outlet is kept constant at $26\delta^0_\omega$. To reduce the noise from the inlet such that it is negligible in comparison to the expected dominant acoustic field, the width of the window-inlet has to be at least $10.5 \cdot \delta^0_\omega$ which is about the distance δ^0_s of two vortices, entering the near field. This result emanates from fig. 7, where the relative error of the different far fields, based on a far field with a wide window-inlet, is plotted over the window-width b_v.

A comparison between the DNS data and the *Lighthill*-solution is not feasible for this test case since the far field of the DNS is superposed by noise from the region of the forcing and the expected sound from the vortex

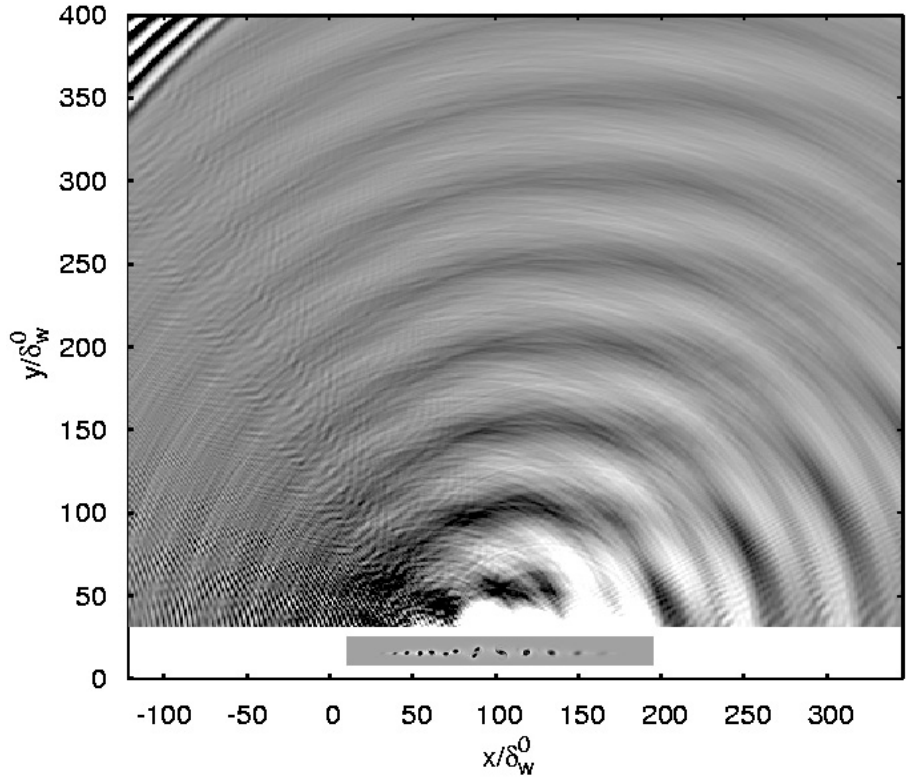

FIGURE 4. Acoustic far field; computed with Lighthill's analogy, pressure fluctuation ± 5 [Pa], WENO-4. The top left-hand corner of the figure is physically incorrect because of missing time steps in the past of the mixing layer.

pairing is not visible. However, the *Lighthill*-solution is predicting the dominant acoustic noise source of the vortex pairing with the expected frequency. In the following test case a comparison between the DNS and the analogies is presented.

3.2. **Supersonic mixing layer with shock**

In this test case shock-induced noise is investigated. This is achieved by a turbulent sub-/supersonic mixing layer with an impinging oblique shock. In contrast to the above discussed subsonic case, the mixing layer of this test case is only forced by its most unstable frequency f_0 to avoid a vortex pairing. As we will see, a vortex pairing occurs downstream of the interaction point between shock tip and mixing layer, anyway. Although this pairing emits a louder acoustic wave than the shock interaction, it won't disturb us because shock-induced noise is emitted mainly in the upstream direction and the noise of the supersonic vortex pairing in the downstream direction (see fig. 8 (*left*) for details). In fig. 8 (*right*) the full Lighthill source including the acoustic far field of the DNS is visualized. The shock-induced noise is clearly visible in the upstream direction.

For the interpolation of the source at the retarded time their temporal evolution is important. The source is stored with a temporal resolution of $\Delta t = 1/(16 \cdot f_0)$. This seems to be a sufficient condition to satisfy the Nyquist-criterion and to guarantee a physical correct reconstruction of the source (see also fig. 9).

This chapter is closed with the solutions of the analogies (Lighthill/FWH) and the LEE propagation and their comparison to the DNS of this test case. Again, a direct comparison is not possible because the DNS is

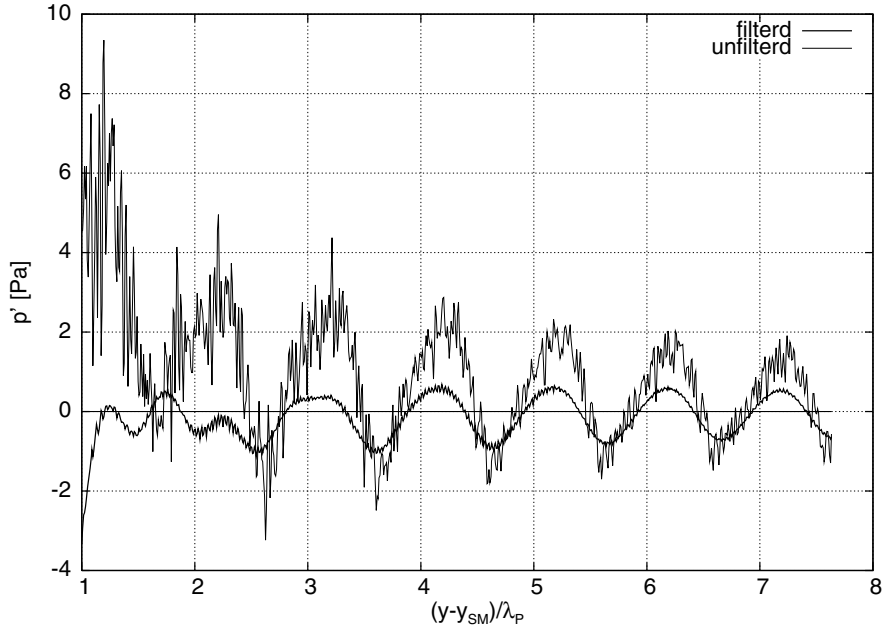

FIGURE 5. Cut through the far field in y-direction at $x = 100\delta^0_\omega$ divided by the wavelength λ_P and measured from the middle of the mixing layer y_{SM}; filtered and unfiltered case.

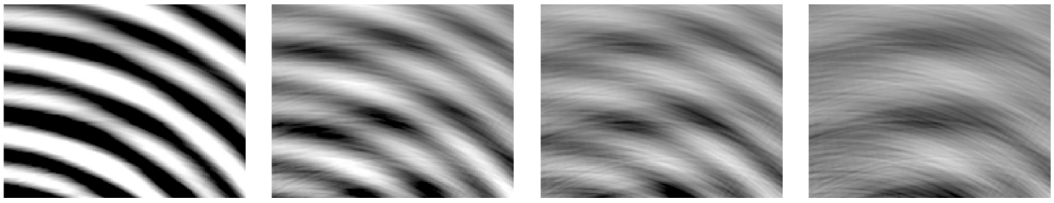

$0\delta^0_\omega$ $2.6\delta^0_\omega$ $6.5\delta^0_\omega$ $13\delta^0_\omega$

FIGURE 6. Far field for different parameters of the window function. Modified is the width of the window function at the inlet, while the width of the outlet is kept constant at 20%. Same color scaling for all cases (± 5.0 [Pa])

CASE			II
u_1	$1.44 \cdot c_0$	L_x/δ^0_ω	346
u_2	$0.216 \cdot c_0$	L_y/δ^0_ω	85
μ_0	$8.365 \cdot 10^{-3} \frac{kg}{m \cdot s}$	n_x	512
$\mathrm{Re}_{\delta^0_\omega}$	$1.90 \cdot 10^3$	n_y	384

TABLE 2. Parameters of the DNS for the mixing layer with shock.

calculating the total pressure and the analogies only the pressure fluctuation. So the ambient pressure p_0 has to be subtracted from the DNS data.

Such a comparison has been performed in fig. 11. The *Lighthill*-solution on the top right hand side of the figure includes the acoustic sources in the near field and the pressure fluctuations in the far field. Only small

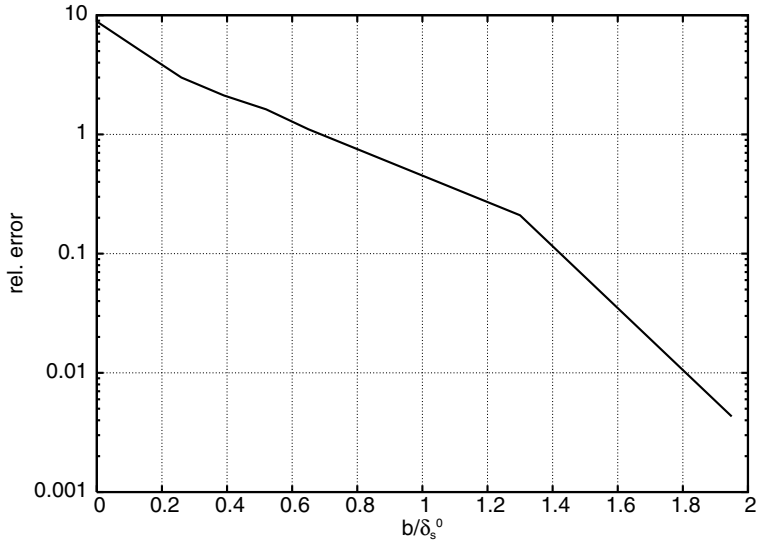

FIGURE 7. Relative error of different far fields (fig. 6), based on a far field with a wide window-inlet, plotted over the window width b_v divided by the distance δ_s^0 of two entering dominant acoustic sources (vortices)

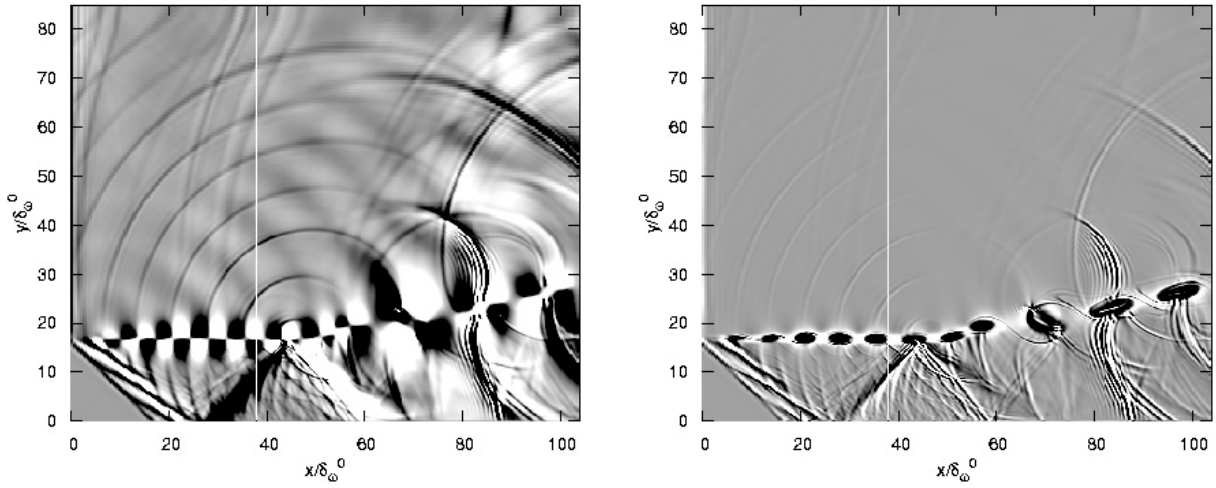

FIGURE 8. *Left:* Instantaneous dilatation field for the mixing layer with shock (DNS); color scale $\pm 100\,[1/s]$; *Right:* Instantaneous field of the full Lighthill source for the same case (DNS); color scale $\pm 5{\cdot}10^6\,[kg/(s^2m^3)]$

qualitative differences to the DNS can be seen in this visualization. Both amplitude and position of the two calculations are in good accordance to each other. In a cut through the far field the differences can be seen more detailed (fig. 12). A high frequency noise superposes the far field of the *Lighthill*-solution and is most dominant in the near of the mixing layer ($y/\delta_\omega^0 < 40$).

The strong derivation of Lighthill's analogy, as it is shown in fig. 12, is not clearly understood. However, one main reason for this discrepancy might be the strong refraction effect of the acoustic signal in the region of

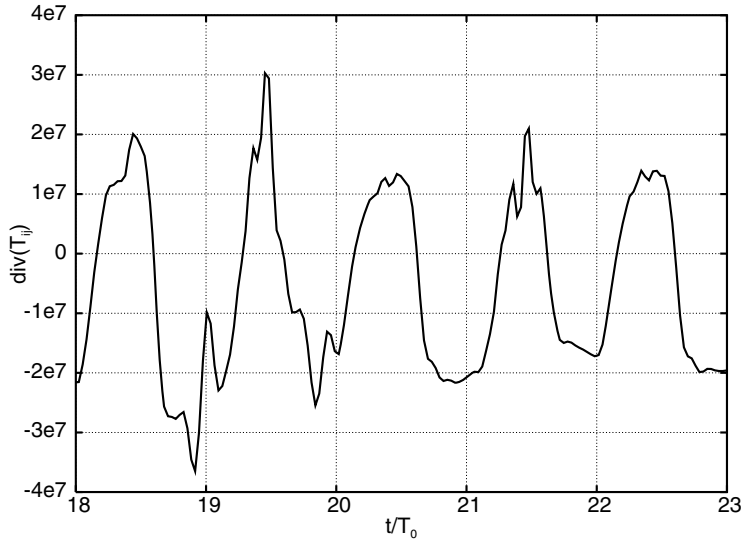

FIGURE 9. Temporal evolution of the full Lighthill source ($\frac{\partial^2 T_{ij}}{\partial x_i \partial x_j}$) measured at the interaction point of shock tip and mixing layer over five periods T_0

the acoustic relevant sources. This refraction effect is particularly dominant in the case of the sub-/supersonic mixing layer with shock. Lighthill's analogy, with the use of a Green's function, is not taking these effects into account, since the speed of sound is expected to be constant in the whole computational domain (see eq. (2.3)). Similar to the method used for the derivation of eq. (2.9), the information of the local speed of the acoustic signal should be included in such an analysis (like a modified retarded time). These effects are negligible for the FWH and the LEE method since the used sources are already in the acoustic far field where a constant speed of the acoustic wave propagation can be assumed (except for the effects of a parallel meanflow, see eq. (2.9)).

The solution for the FWH-method is presented in fig. 11 (bottom right). It includes the acoustic pressure fluctuation in the far field and a part of the source ($\frac{\partial}{\partial t}(\rho v)$, DNS) in the near field. For this two dimensional case, the surface integration turns into a one dimensional problem, so the sources have to be stored only on a line (red line in the near field of fig. 11). This "source-line" has to be placed on an appropriate location in the near field, which should be in general far away from any aerodynamic perturbations. To specify this place more precisely, a parameter study with a varying position of the source-line in y-direction has been performed. The resulting far fields of each different source-line are then compared to the far field of the source-line with the largest distance to the mixing layer and their relative error is identified. In addition to this we use the Q-criterion of Hunt et al. [22], which defines the zones where rotation is predominant, to measure the strength of the aerodynamic perturbations:

$$Q = \frac{1}{2}[r_{ij}r_{ij} - s_{ij}s_{ij}], \tag{3.17}$$

with the strain rate tensor s_{ij} and the rotation tensor r_{ij}. In fig. 10 both the L_2-norm of the Q-criterion and the above mentioned relative error are plotted with a logarithmic scaling (to compare both curves an arbitrary scaling is used). It can be shown that the Q-criterion is linked to the relative error and therefore acts as an indicating value for the positioning of the source-line. In our case the source-line is well placed in a distance to the mixing layer of at least $20\delta^0_\omega$. In addition to this we can see that the position of the FWH-surface ("source-line") is not sensitive, since the relative error is constant once we are in the acoustic far field.

A comparison to the acoustic far field of the DNS is included in fig. 12. Apart from the superposed pressure decay in the DNS, the amplitude, wavelength and the shape of the waves are in good accordance to the DNS. The numerical noise in the FWH-far-field is negligible in comparison to Lighthill's analogy.

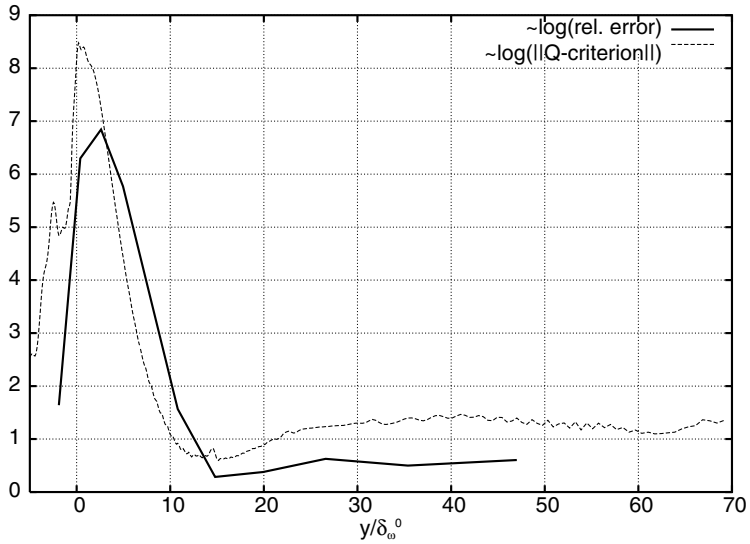

FIGURE 10. Comparison of the Q-criterion (L_2-norm) and the relative error between the far fields for different positions of the stored sources. Center of the mixing layer at $y = 0\delta_\omega^0$

The results of the linearized Euler Equations are presented in fig. 11 (bottom left) and, in a comparison to the DNS and the analogies, in fig. 12. The results seem to match with the ones of the DNS.

4. Concluding remarks

The *Lighthill/FWH*-code is implemented to evaluate the sound emitted by the Lighthill/FWH-sources with an integral formulation. Different numerical schemes for the treatment of the source are tested to determine their influence to the numerical solution, like the influence of the window function, the filtering and averaging of the source and different interpolation procedures. In addition to this, we compared the the results to the LEE propagation.

A two-dimensional subsonic mixing layer was used as a first application case for the Lighthill-sources. Although we observed a superposition of spurious high frequency noise in the far field of the Lighthill solution, the dominant frequency of the vortex pairing could be identified. The expected sound in the DNS was not clearly visible in this "small" computational domain, so no direct comparison to the DNS was possible. In order to minimize high frequency noise in the far field, low pass filtering of the sources was necessary.

second test case was used to investigate shock-induced noise with the Lighthill- and the FWH-method and also the LEE. It could be shown that the accordance between the FWH-method and the DNS was much better than the one of Lighthill's solution. Close to the near field the differences between the DNS and Lighthill's analogy were most dominant. Far away from the aerodynamic fluctuations, the position and the frequency of the acoustic waves in Lighthill's analogy match with the ones of the DNS, although the amplitude differs. Again, high frequency noise superposed the solution of both analogies. With a parameter study, the L_2-norm of the Q-criterion was found to be an indicating value for an appropriate position of the source-surface in the FWH-method. This value seems to be an important parameter to optimize the hybrid simulation.

In a comparison to the DNS, the solution of the FWH-method was not only better than the Lighthill-method, but also much faster. The FWH method reached its solution at least 30 times faster than Lighthill's analogy. This is important for computational expensive three-dimensional cases. In addition to this the amount of storage decreases for the FWH-method since the sources are stored on a surface and not in a volume, although one needs to save a tensor instead of a scalar. However, the most important advantage of the FWH-method,

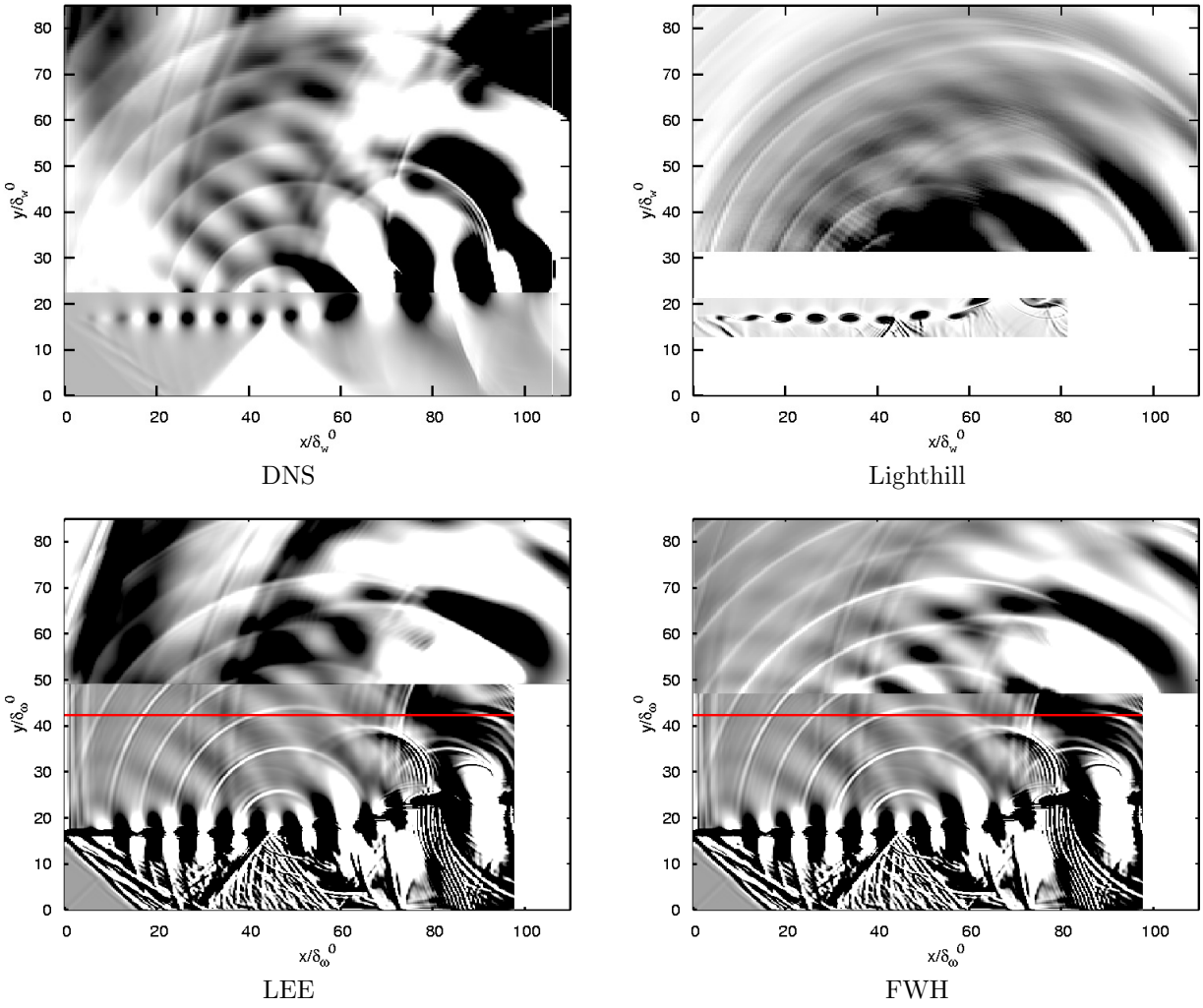

FIGURE 11. Comparison of all used numerical prediction methods. *Top left:* DNS, ($p'[\pm 600$ Pa]) (for a more descriptive visualization, the area around the mixing layer has a different color scaling ($p'[\pm 12000$ Pa]). *Top right:* Lighthill solution, ($p'[\pm 600$ Pa]), including the source-area in the near field ($\frac{\partial^2 T_{ij}}{\partial x_i \partial x_j}$). *Bottom left:* LEE propagation, ($p'[\pm 600$ Pa]), far field starts at $y/\delta_\omega^0 \approx 50$, the near field shows a part of the FWH-source ($\frac{\partial}{\partial t}(\rho v)$) $[\pm 3 \cdot 10^3]$. The red line denotes the location of the variables, used as input data for the LEE-code. *Bottom right:* FWH-solution, far field starts at $y/\delta_\omega^0 \approx 50$, near field shows a part of the FWH-source ($\frac{\partial}{\partial t}(\rho v)$) $[\pm 3 \cdot 10^3]$. The red line denotes the location of the sources, used as input data for the FWH-code.

in relation to Lighthill's analogy, is that a modification of the sources like windowing, filtering or averaging is needless. The results of the LEE reproduce the overall shape of the near acoustic field provided by the DNS. In comparison to the analogies, no high frequency noise is visible in the solution of the LEE-propagation.

Even though the analogies differ from the DNS, it could be shown that Lighthill's analogy and especially the FWH- and the LEE-method have the ability to predict shock-induced noise.

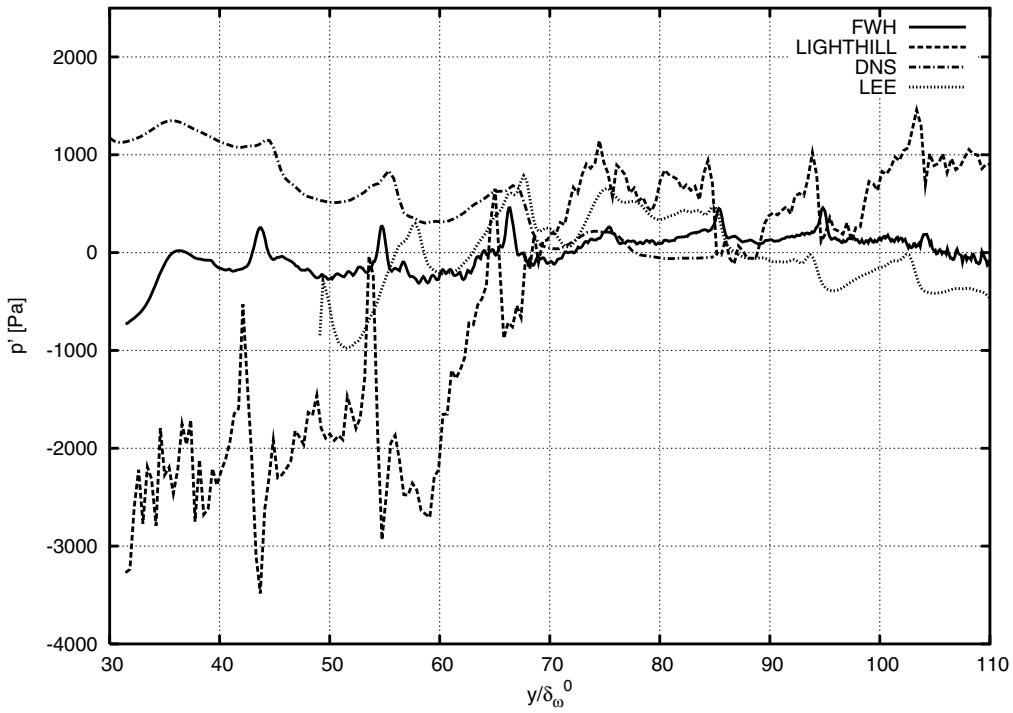

FIGURE 12. Comparison of the analogies (Lighthill/FWH) and the LEE-propagation to the DNS, Pressure-fluctuation.

REFERENCES

[1] Andersson, N., Erikson, L., Davidson L. (2004). A Study of Mach 0,75 Jets and Their Radiated Sound Using Large-Eddy Simulation. *10th AIAA/CEAS Aeroacoustics Conference (2004)*

[2] Bailly, C. and Juvé, D. (2000). Numerical solution of acoustic propagation problems using linearized Euler equations. *AIAA J. 38(1):22-29*

[3] Bailly, C., Bogey, C. (2004). Contributions of computational aeroacoustics to jet noise research and prediction. *Int. J. of Comp. Fluid Dynamics 18(6):481-491*

[4] Berland J., Bogey C. and Bailly C., (2006). Low-dissipation and low-dispersion fourth-order Runge-Kutta algorithm. *Comput. Fluids.*

[5] Berland J., Bogey C. and Bailly C., (2006). Large eddy simulation of screech tone generation in a planar underexpanded jet. *12th AIAA/CEAS Aeroacoustics Conference*, 8-10 May, Cambridge, Massachusetts, USA. AIAA Paper 2006-2496.

[6] Bogey, C. Bailly, C. and Juvè, D. (2000). Numerical simulation of sound generated by vortex pairing in a mixing layer. *AIAA Journal 38(12):2210-2218*

[7] Bogey, C. Bailly, C. and Juvè, D. (2001). Noise computation using Lighthill's equation with inclusion of mean flow - acoustic interaction. *AIAA Paper 2001-2255*

[8] Bogey, C., Gloerfelt, X. and Bailly, C. (2003). Illustration of the inclusion of sound-flow interactions in Lighthill's equation. *AIAA J. 41(8):1604-1606*

[9] Bogey C. and Bailly C. (2004). A family of low dispersive and low dissipative explicit scheme for flow and noise computations. *J. of Computational Physics 194:194-214.*

[10] Colonius, T., Lele, S. and Moin, P. (1997). Sound generation in a mixing layer. *J. of Fluid Mech. 300:575-409*

[11] Colonius, T., Mohseni, K., Freund, J., Lele, S. and Moin, P. (1998). Evaluation of noise radiation mechanisms in a turbulent jet. *Center for Turbulence Research 1998*

[12] Crighton, D. G. (1975). Basic principles of aerodynamic noise generation. *Prog. Aerospace Sci., 16(1):31-96*

[13] Hardin, J. C. and Hussaini, M. Y. (1993). Computational aeroacoustics for low Mach number flows. *Computational Aeroacoustics, Springer Verlag (1993) S. 50-68*

[14] Ehrenfried, K. (2003). Strömungsakustik I. *Vorlesungsskript. Technische Universität Berlin.*

[15] Ehrenfried, K. (2003). Strömungsakustik II. *Vorlesungsskript. Technische Universität Berlin.*
[16] Farrasat, F., Doty, M. and Hunter, C. (2004). The acoustic analogy - a powerfull tool in aeroacoustics with emphasis on jet noise prediction. *10th AIAA/CEAS Aeroacoustics Conference , Manchester, United Kingdom, May 10-12, 2004*
[17] Farrasat, F. and Posey, J. W. (2003). The role of analytic methods in computational aeroacoustics. *International Journal of Aeroacoustics 1(3):207-240*
[18] Friedrich, R. (2002). Kompressible Strömungen mit Reibung und Wärmeleitung. *Fachgebiet Strömungsmechanik. Technische Universität München.*
[19] García, A. (2004). Weighted ENO y aplicationes. *Departamento de Mathemática Aplicada. Universitat de Valéncia (Spain)*
[20] Goldstein, M. E. (1976). Aeroacoustics. *McGraw-Hill, New York, 1976*
[21] Hoare, C. A. R. (1962). QuickSort. *Computer Journal 5(1):10-15*
[22] Hunt, J. C. R., Wray, A. and Moin, P. (1988). Eddies, stream, and convergence zones in turbulent flows. *Center for Turbulence Research Report CTR-S88*
[23] Juvé, D. (2004). Two topics in computational aeroacoustics. *DFG-CNRS Seminar, Orléans, september 6-7, 2004*
[24] Lighthill, M. J. (1952). On sound generated aerodynamically-I. General theory. *Proceedings of the Royal Society of London 221(A 1107):564-587*
[25] Lilley, G. (1974). On the noise from jets. *AGARD CP-131 pp. 13.1-13.12*
[26] Liu, X., Osher, S. and Chan, T. (1994). Weighted Essentially Non-oscillatory Schemes. *J. of Computational Physics 115:200-212*
[27] Manning, T. (1999). A numerical investigation of sound generation in supersonic jet screech. *PhD thesis. Department of aeronautics and astronautics. Stanford University*
[28] Michalke, A. (1964). On the inviscid instability of the hyperbolic-tangent velocity profile. *J. of Fluid Mech. 19:543-556*
[29] Mitchelle, B., Lele, S. and Moin, P. (1999). Direct computation of the sound generated by vortex pairing in an axisymmetric jet. *J. of Fluid Mech. 383:113-142*
[30] Morris, J, Farassat, F. (2002). Acoustic analogy and alternative theories for jet noise prediction. *AIAA J. 40(4):671-680*
[31] Powell, A. (1953). On the mechanism of choked jet noise. *Proceedings of the Royal Society of London B, 66:1039-1056*
[32] Powell, A. (1953). On the noise emanating from a two-dimensional jet above the critical pressure. *Aeronautical Quaterly, 4(2):103-122*
[33] Powell, A. (1954). The reduction of choked jet noise. *Proceedings of the Royal Society of London B, 67(4):313-327*
[34] Rembold, B., Freund, J. and Wang M. (2002). An evaluation of LES for jet noise prediction. *Center for Turbulence Research. Proceedings of the Summer Program 2002.*
[35] Rembold, B. (2003). Direct and large-eddy simulation of compressible rectangular jet flow. *PhD thesis. Swiss Federal Institute od Technology Zrich.*
[36] Rienstra, S. and Hirschberg, A. (2002). An introduction to acoustics. *Eindhoven University of Technology.*
[37] Schaupp, C. (2004). Numerische Untersuchung stossinduzierten Lärms. *Diplomarbeit, Fachgebiet Strömungsmechanik, Technische Universität München, 2004*
[38] Sebastian, K., Shu, C. (2003). Multidomain WENO finite difference method with interpolation at subdomain interfaces. *Journal of Scientific Computing 19,Nos 1-3*
[39] Sesterhenn, J. (2001). A characteristic-type formulation of the Navier-Stokes equations for high order upwind schemes. *CAF 30(1):37-67*
[40] Shu, C. 2003. High-order finite difference and finite volume WENO schemes and discontinous Galerkin methods for CFD. *Int. J. of Comp. Fluid Dynamics 17(2):107-118*
[41] Tam, C. K. W., Ahuja, K. K., Jones, R. R. (1994). Screech tones from free and ducted supersonic jets. *AIAA J., 31(5):917-922*
[42] Tam, C. K. W.(1995). Computational aeroacoustics: Issues and methods. *AIAA J. 33(10):1788-1796*
[43] Tam C.K.W. and Dong Z. (1996). Radiation and outflow boundary conditions for direct computation of acoustic and flow disturbances in a nonuniform mean flow. *J. of Computational Acoustics 4(2):175-201.*
[44] Numerical simulation of flow-induced noise by means of the hybrid method with LES and aeroacoustic analogy. *Dissertation. Fachbereich Maschinentechnik der Universitt Siegen.*
[45] Wang, M., Lele, S. and Moin, P. (1996). Computation of quadrupole noise using acoustic analogy. *AIAA J. 34(11):2247-2254*